



International Journal of Abrasive Technology

ISSN online: 1752-265X - ISSN print: 1752-2641

<https://www.inderscience.com/ijat>

An investigation on tool wear rate in the electrical discharge face grinding process for the machining of Monel 400

Akshat Srivastava Kulshrestha, Mandeep Singh, Deepak Rajendra Unune, Ashok Kumar Dargar

DOI: [10.1504/IJAT.2023.10053479](https://doi.org/10.1504/IJAT.2023.10053479)

Article History:

Received:	20 April 2022
Accepted:	27 November 2022
Published online:	12 May 2023

An investigation on tool wear rate in the electrical discharge face grinding process for the machining of Monel 400

Akshat Srivastava Kulshrestha,
Mandeep Singh, Deepak Rajendra Unune*
and Ashok Kumar Dargar

Department of Mechanical-Mechatronics Engineering,
The LNM Institute of Technology,
Jaipur-302031, India

Email: 18pmm002@lnmiit.ac.in

Email: 18pmm003@lnmiit.ac.in

Email: deepak.unune@lnmiit.ac.in

Email: ashok.dargar@lnmiit.ac.in

*Corresponding author

Abstract: This paper attempts to model the electrical discharge face grinding (EDFG) process, while machining the Monel 400 superalloy, using the response surface methodology (RSM) and artificial neural network (ANN) for process performance prediction. Initially, the experiments were designed using the central composite design of RSM. The grinding wheel speed, peak current, pulse-on-time, and pulse-off-time were chosen as input process parameters, while tool wear rate (TWR) as the performance attributes. Analysis of variance was to identify the significant model terms and their influence on TWR. The grinding wheel speed was identified as the most influencing parameter, and a 61% reduction in TWR was recorded when increasing the speed from 200 rpm to 600 rpm. The developed ANN model (4-20-1) reduced the mean square prediction error up to four times, outperforming the RSM model.

Keywords: electrical discharge face grinding; tool wear rate; TWR; modelling; artificial neural network; ANN; response surface methodology; RSM; average surface roughness; ASR.

Reference to this paper should be made as follows: Kulshrestha, A.S., Singh, M., Unune, D.R. and Dargar, A.K. (2023) 'An investigation on tool wear rate in the electrical discharge face grinding process for the machining of Monel 400', *Int. J. Abrasive Technology*, Vol. 11, No. 3, pp.196–211.

Biographical notes: Akshat Srivastava Kulshrestha is currently a PhD student at the Department of Mechanical-Mechatronics Engineering at The LNM Institute of Technology, Jaipur (India). He graduated in Mechanical Engineering (2013) from Uttar Pradesh Technical University and obtained his post-graduate degree from Manipal University, Jaipur (2016). After the completion of his Master's degree, he is motivated to pursue PhD and subsequently, a career in research. His diverse research interests include unconventional machining, optimisation and decision-making, and materials characterisation.

Mandeep Singh is currently pursuing a PhD in Mechanical Engineering from The LNM Institute of Information Technology. He received his Masters in Technology in Machine Design from Rajasthan Technical University, Kota. His current research interests are IC engines, biofuels, renewable energy, microalgae, FEA, optimisation, ANN, etc.

Deepak Rajendra Unune is currently working as an Assistant Professor in the Department of Mechanical-Mechatronics Engineering at The LNM Institute of Technology, Jaipur (India). Previously, he received the prestigious ‘Marie Skłodowska-Curie Actions Individual Fellowship’ from European Commission. He was invited for two years (2019–2021) of post-doctoral research work at the Department of Materials Science and Engineering at the University of Sheffield, UK. He was awarded a PhD by the Malaviya National Institute of Technology, Jaipur, India, in 2016. He has more than nine years of teaching and research experience and more than 50 research publications in peer-reviewed journals and conferences. His areas of interest include CNC machining of advanced materials, micro-machining, sustainable manufacturing, EDM, Micro-EDM, submerged arc welding, surface treatments of biomaterials, etc.

Ashok Kumar Dargar is currently working as an Associate Professor at The LNM Institute of Information Technology, Jaipur, India. He obtained his PhD in synthesising and analysing kinematic chains and mechanisms from Jamia Millia Islamia University, Delhi, India. He has published and presented more than 30 research papers in international journals and conferences. His current research areas include synthesis and analysis of kinematic chains, mechanisms, stress analysis, condition-based monitoring, optimisation of process parameters, and hybrid machining.

1 Introduction

Electrical discharge grinding (EDG) is a hybrid electrical discharge machining (EDM) process that unites spark erosion of EDM and mechanical abrasion action of grinding for material removal purposes (Singh et al., 2010; Unune and Mali, 2017). EDG delivers higher material removal and better surface quality than the conventional EDM process (Shu and Tu, 2003). EDG employs an electrically conductive disc-shaped rotary tool or grinding wheel in contrast to the stationary tool in the case of die-sink EDM. The benefit of adopting a rotary tool is that the tool wear can be well distributed to the disk or grinding wheel surface. The rotary motion of the tool effectively removes the debris particles and molten metal in the inter-electrode gap between the tool and the workpiece. Typically, EDG can be done in three configurations:

- 1 electrical-discharge face grinding (EDFG)
- 2 electrical-discharge cut-off grinding (EDCG)
- 3 electrical-discharge surface grinding (EDSG) (Unune et al., 2016).

The flat face side of the grinding wheel, when performing machining in EDG, such setup is termed as EDFG. The grinding wheel rotates around the spindle axis and feeds perpendicular towards the machine table (Abothula et al., 2010). Yadav et al. (2015) developed the EDFG setup and, through the experimental analysis, claimed that EDFG

attributed to enhanced material removal rate (MRR) and average surface roughness (ASR). The EDFG performance is characterised by maximum MRR, lower tool wear rate (TWR), and reduced ASR. Tyagi et al. (2017) performed the EDFG process. They studied the influence of input process parameters such as grinding wheel speed (GWS), T_{on} , T_{off} , and peak current (I_p) on MRR, ASR, and wheel wear rate (WWR). They used a multi-response signal-to-noise (S/N) ratio and analysis of variance (ANOVA) to evaluate the process performance. The calculation for WWR was done using the 'smaller the better' approach, and the optimal values of process parameters for WWR are derived as I_p at 3 A, T_{on} at 100 μ s, T_{off} at 75 μ s, and GWS at 925 rpm. The experimental investigation has confirmed the validity to enhance machining performance and optimise process conditions in EDFG.

Gupta and Tyagi (2017) found that MRR, TWR, and ASR increased with an increase in the I_p , GWS , and T_{on} . The most significant factor affecting the EDFG robustness was I_p and T_{on} . It was also found that the size of the crater decreases with an increase in GWS . Yadav and Yadava (2017) performed electrical discharge diamond grinding (EDDG), and they predicted TWR and ASR for the process using artificial neural network (ANN). The input parameters were I_p , duty ratio, GWS , and grain size. They stated that I_p , duty ratio, GWS , and grain size ranges should be low for minimum TWR.

The literature review found that rare work is reported on the study of TWR during the EDFG process for machining nickel-based superalloys (Monel-400). In addition, EDFG has a complex nature. Thus, applying predicting modelling techniques like response surface methodology (RSM) and ANN would enable the industry to accurately predict the process performance. Therefore, in the current work, the central composite design (CCD) design of experiments approach was initially used to plan and perform the EDFG of Monel-400. The process parameters were GWS , I_p , T_{on} , and T_{off} , while TWR was chosen as the response variable. RSM and ANN models were developed to predict the TWR. Then the ANN and RSM models prediction performance were compared with the validation experiments.

2 Processing principle and method

2.1 Response surface methodology

RSM is an empirical mathematical modelling technique that seems critical in assessing the correlation among numerous process parameters and their responses to specific criteria. As a result, the relevance of the process parameters is determined (Kumar et al., 2017). However, RSM is a statistical and numerical approach that predicts and optimises response parameters. Tangible independent variables impact the response demand (Singh et al., 2014; Unune et al., 2019).

In complex interactions, RSM could assess the relative importance of various factors. It is a valuable strategy for examining multiple process variables because it requires minimal experimental trials versus studying one variable at a time. RSM provides an answer to choosing the applied factors levels to attain the response desired value in the minimum number of experiments. RSM independent process parameters for analysis can be represented as the equation (1).

$$Y = a_0 + \sum_{i=1}^n a_i x_i + \sum_{i=1}^n a_{ii} x_i^2 + \sum_{i=1}^n a_{ij} x_i x_j \quad (1)$$

Y is output, a_0 coefficients for the unrestricted terms, a_i coefficients for linear terms, a_{ii} coefficients for quadratic terms, and a_{ij} coefficients for the interface terms.

2.2 Artificial neural network

ANN comprises interconnected neurons and shares some characteristics with biotic neurons. ANN is an indication processing paradigm encouraged by biological nervous system procedures. Neural networks are nonlinear structures composed of simple processors termed neurons interrelated by weighted connections. The neuron receives input and produces an output that can be seen as a replication of local information stored in connections (Davim et al., 2008). The flow chart that provides the principle of the ANN algorithm is shown in Figure 1. Therefore, we used the computational capability of a multi-layered neural network for interpretation and to predict TWR involved in machining Monel 400 during the EDFG process.

ANN operates in the same manner as a ‘black box’ model, requiring no detailed system knowledge. Instead, they learn about the link between the input factors and the regulated and uncontrolled variables by reviewing previously recorded data, much like a nonlinear regression. An ANN is capable of mimicking the behaviour of organic neural networks. In general, an ANN is formed of neurons linked together. A gradient descent strategy, also known as the backpropagation learning scheme, reduces the network mean square error (MSE) in this fully connected, feed-forward design. For reliable predictions, back-propagation neural networks using the Bayesian regularisation learning algorithm are typically used as it improves the generalisation and minimises the overfitting of the trained networks (Gouravaraju et al., 2021). Equation (2) judged the networks performance based on the MSE.

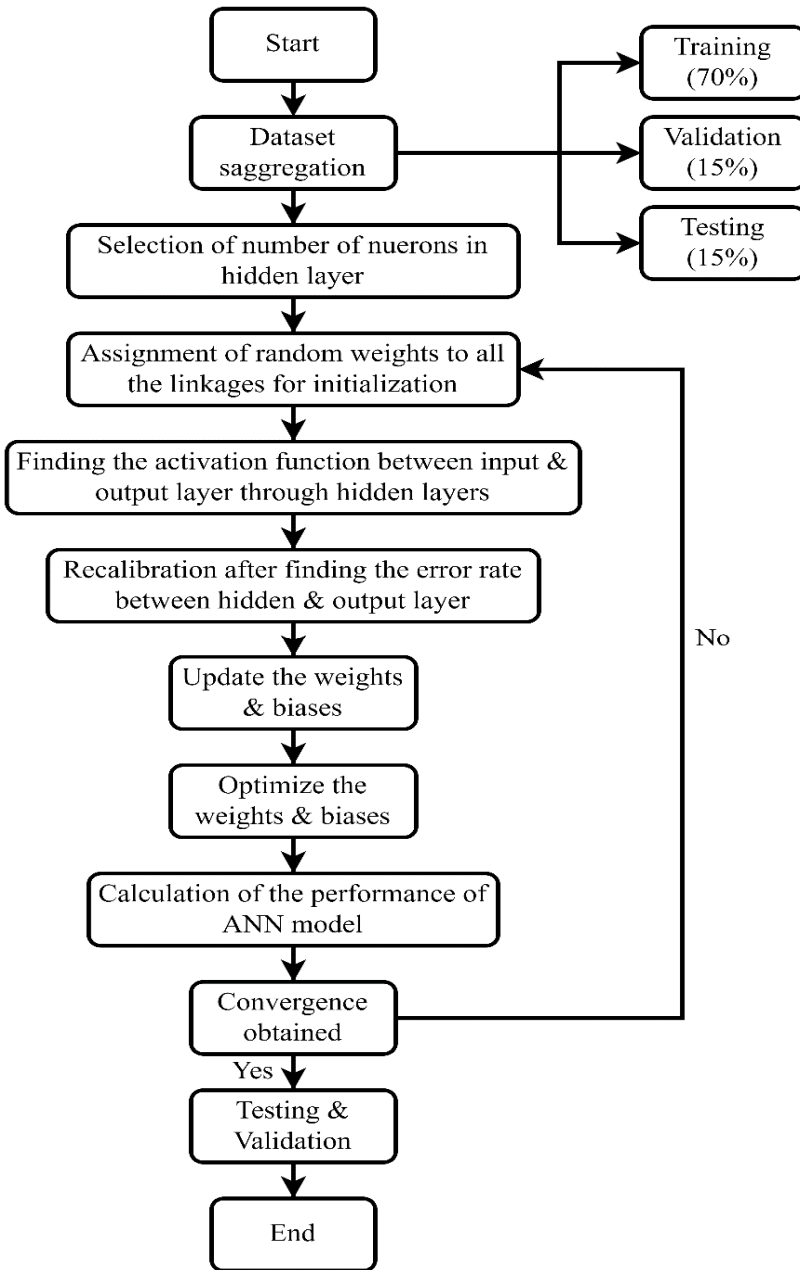
$$MSE = \frac{1}{A \times B} \sum_{j=1}^B \sum_{i=1}^A (Y'_p - Y_p)^2 \quad (2)$$

where experimental output of the i^{th} neuron, predicted output of the i^{th} neuron, B is the total number of training arrays, and A is the overall number of neurons in the output layer (Youssefi et al., 2009).

Equation (3) was used to calculate the coefficient of correlation, R^2 (relation between actual and predicted values) of the model

$$R^2 = 1 - \left(\frac{\sum_{i=1}^n (ti - Oi)^2}{\sum_{i=1}^n (Oi)^2} \right) \quad (3)$$

Figure 1 Principle of ANN algorithm



3 Experimentation and test conditions

Experimentation was carried out on the EDM machine (ELTECH-D300), as shown in Figure 2, with an integrated EDFG attachment, as shown in Figure 3(a), and the schematic view of the EDFG setup shown in Figure 3(b). Each experiment was performed for 30 minutes before evaluating the response parameter. The experimental planning of four process parameters with their selected levels is shown in Table 1. Figure 4 depicts the modelling approach used to predict the TWR.

Figure 2 Photograph of EDM machine (see online version for colours)

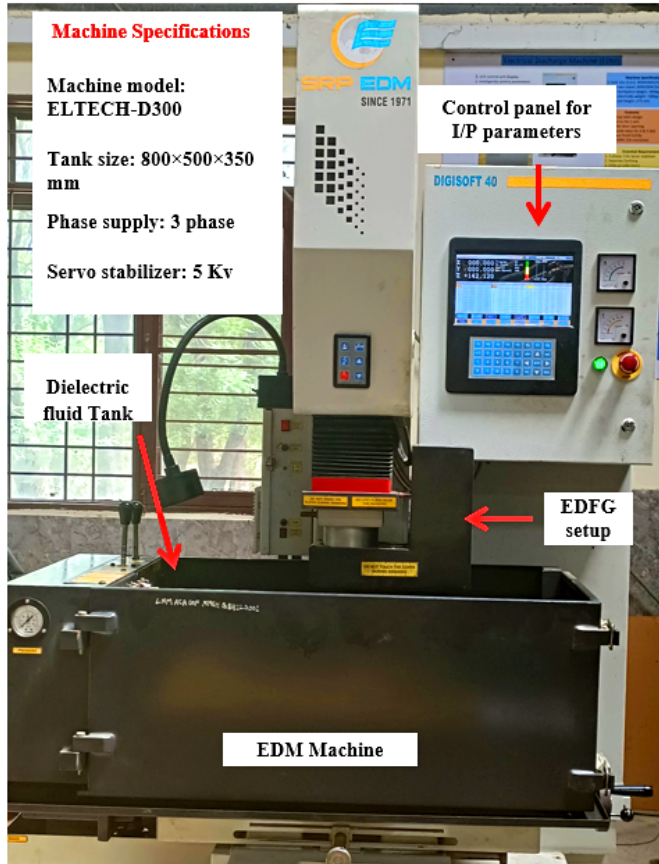


Table 1 Experimental input parameters and their levels

Levels	GWS (rpm)	I_p (A)	T_{on} (μs)	T_{off} (μs)
1	200	5	50	4
2	400	10	75	7
3	600	15	100	10

Figure 3 Electrical discharge face grinding, (a) photograph (b) schematic (see online version for colours)

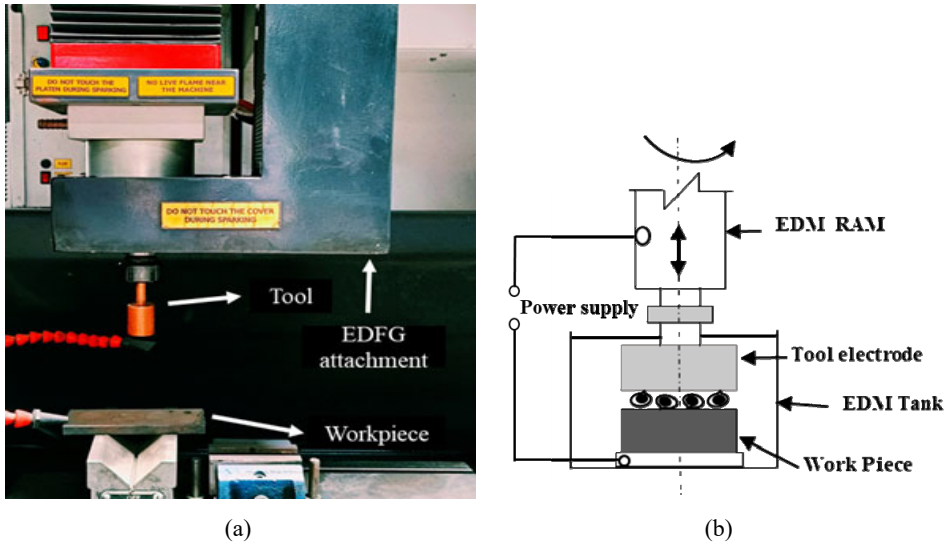
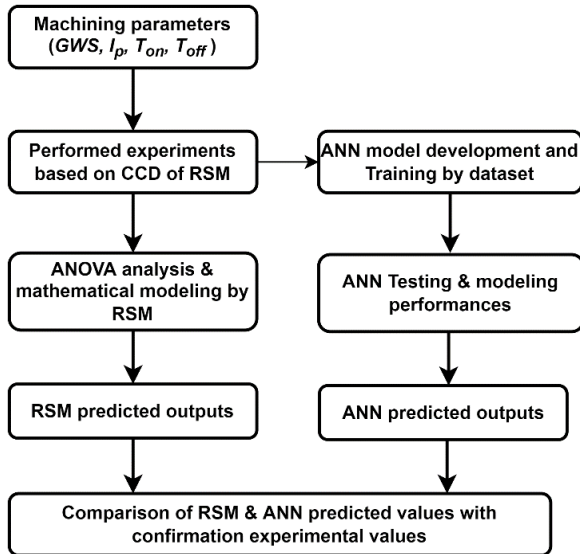


Figure 4 Preparation for the modelling approach



3.1 Workpiece material and grinding tool

Model 400, nickel-copper superalloy, known as difficult-to-cut material, was used as the workpiece in this work. Monel 400 is resistant to a wide range of corrosive conditions and has excellent strength and toughness. Shoemaker and Smith (2006) stated that Monel 400 was frequently employed in the marine and chemical processing industries. Furthermore, nickel-based alloys possess excellent corrosion and thermal fatigue

resistance (Unune et al., 2016). The chemical composition for Monel 400 is shown in Table 2. A cylindrical rod of copper diameter 25 mm was used as a grinding wheel for experimentation. The tool length was set at 60 mm.

Table 2 The Monel 400 chemical composition

<i>Elements</i>	<i>Ni</i>	<i>Fe</i>	<i>Mn</i>	<i>Cu</i>	<i>Cr</i>	<i>Mo</i>	<i>Ti</i>
%	65.31	1.76	1.01	30.63	0.83	0.08	0.07

3.2 Measurement of response

All experiments were performed as per the strategy, and then the response TWR was calculated using equation (4).

$$TWR = \frac{(T_{wi} - T_{wf}) \times 1,000}{\rho \times t} \quad (4)$$

Here, TWR was measured in mm^3/min . T_{wi} = weight of tool prior-machining, T_{wf} = weight of tool post-machining, ρ is the density of the tool material, t is the machining time in minutes.

3.3 Response surface methodology

In the present work, the experiments were planned by employing CCD, a well-known design methodology within RSM. This technique minimises the number of experimental trials required to analyse the effects of each parameter and its interactions. The experiments and the measured TWR are shown in Table 3.

Table 3 Experimental plan with process machining parameters

<i>Sr. no.</i>	<i>GWS</i> (<i>rpm</i>)	<i>I_p</i> (<i>A</i>)	<i>T_{on}</i> (μs)	<i>T_{off}</i> (μs)	<i>TWR</i> (mm^3/min)
1	400	10	75	7	0.59
2	400	15	75	7	0.72
3	600	5	100	4	0.41
4	200	10	75	7	0.68
5	600	15	100	10	0.75
6	600	5	50	10	0.52
7	400	10	75	7	0.59
8	200	15	100	10	0.71
9	400	10	75	7	0.59
10	600	15	100	4	0.49
11	200	10	75	7	0.79
12	400	10	75	7	0.59
13	400	5	75	7	0.52
14	200	15	100	4	0.72
15	200	5	50	4	0.76

Table 3 Experimental plan with process machining parameters (continued)

<i>Sr. no.</i>	<i>GWS</i> (<i>rpm</i>)	<i>I_p</i> (<i>A</i>)	<i>T_{on}</i> (<i>μs</i>)	<i>T_{off}</i> (<i>μs</i>)	<i>TWR</i> (<i>mm³/min</i>)
16	400	10	100	7	0.6
17	600	15	50	10	0.68
18	600	5	50	4	0.37
19	400	10	75	7	0.59
20	600	5	100	10	0.41
21	400	10	75	7	0.59
22	200	15	50	4	0.92
23	400	10	75	4	0.64
24	400	10	75	10	0.64
25	200	5	50	10	0.82
26	400	10	75	7	0.59
27	200	5	100	10	0.68
28	600	15	50	4	0.55
29	200	5	100	4	0.37
30	200	15	50	10	0.94

4 Result and discussion

For the analysis of the experimental data, the Design-Expert 12 software was used. The influence of the process parameters concerning the TWR was investigated using ANOVA analysis. The backward elimination method was utilised to eliminate insignificant terms to improve the model.

4.1 ANOVA for TWR

The ANOVA table for TWR (Table 4) and the model F-value of 32.75 denote that the model is significant. The model terms are significant if their value is less than 0.05, while A, B, and C are significant. The ‘Pred R-Squared’ value of 0.7601 agrees reasonably with the ‘Adj R-Squared’ value of 0.8455. The S/N ratio is measured by ‘Adeq Precision.’ A ratio greater than four is preferred. The ratio of 24.70 suggests a sufficient signal in this case. The lack of fit F-value of 4.79 implies the lack of fit is significant. There is only a 2.13% chance that a lack of fit F-value this large could occur due to noise, and T_{on} was found to be an insignificant process parameter, among others.

4.2 Regression equations

The given quadratic [equation (5)] show the relationships between the input process parameters (GWS , I_p , T_{on} , and T_{off}) and the response characteristic (TWR).

$$TWR = 1.06266 - 0.001390 \times GWS + 0.018000 \times I_p - 0.006952 \times T_{on} + 0.017037 \times T_{off} + 0.000011 \times GWS \times T_{on} \quad (5)$$

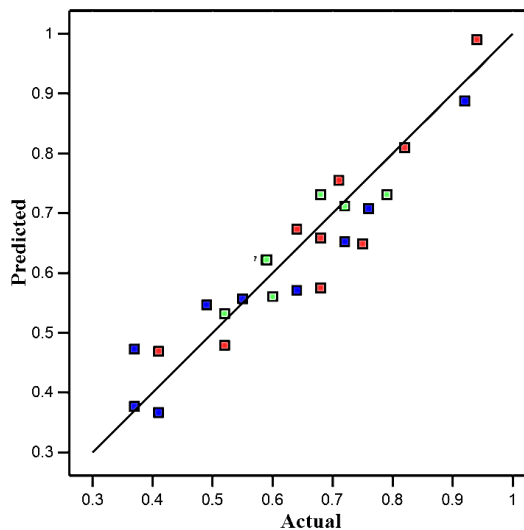
Table 4 ANOVA for TWR

Source	Sum of squares	df	Mean square	F value	p-value prob. > F	contribution
Model	0.521	5	0.1042	32.75	< 0.001	significant
A – GWS	0.213	1	0.2131	66.95	< 0.001	significant 35.65
B – I_p	0.145	1	0.1458	45.81	< 0.001	significant 24.39
C – T_{on}	0.0638	1	0.0638	20.03	0.08	
D – T_{off}	0.047	1	0.0470	14.77	0.002	7.86
Residual	0.076	24	0.0032			
Lack of fit	0.070	17	0.0041	4.79	0.0213	significant
Pure error	0.006	7	0.0009			
Cor. total	0.597	29				
Std. dev.			0.056	R- squared		0.872
Mean			0.627	Adj R- squared		0.845
C.V. %			8.99	Pred R- squared		0.760
Press			0.143	Adeq precision		24.70

4.3 Normal probability plot

Figure 5 depicts the normal probability plot for TWR; most predicted values match the experimental results or values of TWR in (mm³/min), which means the data are regularly distributed with no significant deviances. This shows the effectiveness of the developed model. Similarly, El-Taweel (2009) also proved the developed model effectiveness.

Figure 5 Normal probability plot of TWR (see online version for colours)



4.4 The effect of input process parameters on TWR

Due to the spark heat generated between the tool and the workpiece. As a result, the tool also erodes during machining, affecting the final output. TWR cannot be averted, but it can only be reduced. Figure 6(a)–6(c) illustrates the effect of input parameters on TWR.

Figure 6 The individual effect of process parameters on TWR, (a) effect of GWS on TWR (b) effect of I_p on TWR (c) effect of T_{off} on TWR

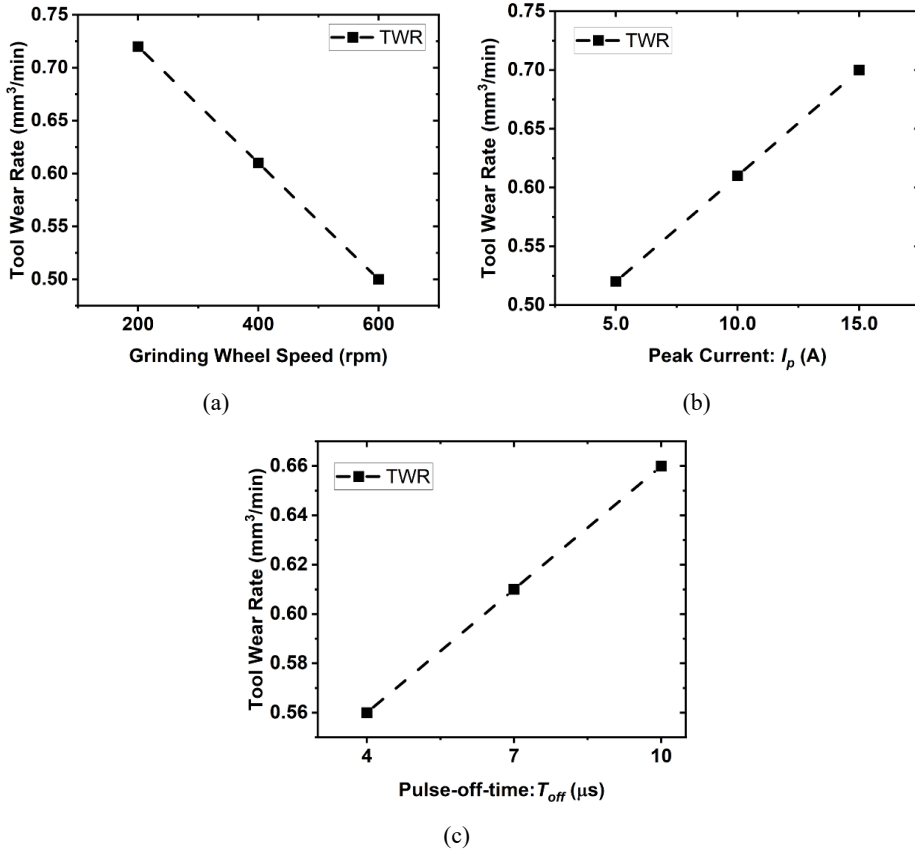
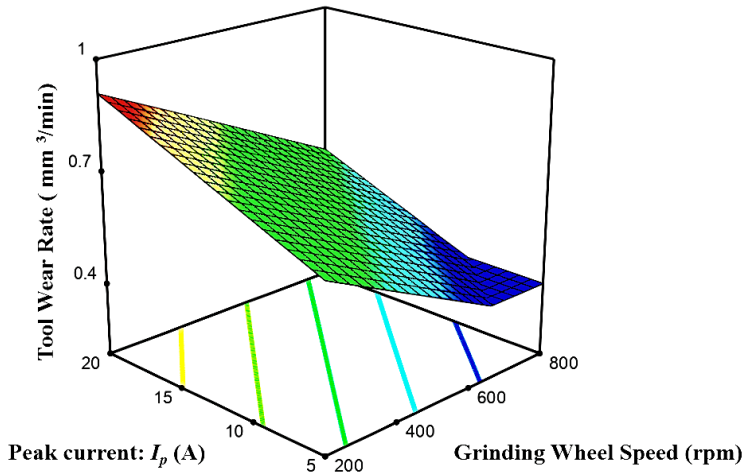


Figure 6(a) depicts a reduction in TWR with every increase in GWS . These reductions are because the centrifugal force increases at each level of GWS , which helps remove the debris suspended in the machining gap facilitated by the flow of dielectric fluid. Figure 6(b) shows the increase in TWR as the level of I_p increases. The I_p is related to the amount of discharge energy, and this discharge energy is divided between the tool, workpiece, and dielectric fluid during machining. The amount of melted and vaporised materials from the tool and workpiece increases as the discharge energy increases. And also, the process parameters setting decides the spark intensity generated or heat supply between the tool and workpiece.

Similarly, Figure 6(c) depicts an increase in TWR as T_{off} increases. When the T_{off} is for a short time, there is insufficient time to remove debris from the inter-electrode gap (IEG), resulting in increased TWR. A similar effect of T_{off} was also cited by Wu et al. (2009) on TWR. The interaction effect plot of GWS and I_p can be seen in Figure 7, and it can be perceived that the decline in TWR can be achieved when the GWS is higher along with a lower value of I_p during EDFG.

Figure 7 Interaction effect plot of GWS and I_p (see online version for colours)



4.5 ANN performances

In the current work, four input parameters (GWS , I_p , T_{on} , T_{off}) and one output parameter (TWR) were considered in ANN modelling. A network with an input layer, a hidden layer, and an output layer was developed to identify a suitable ANN model, as shown in Figure 8. MATLAB was used to train the developed ANN for input-output patterns. The activation function of hidden and output neurons was preferred to be a hyperbolic tangent. The objective was that MSE (minimise the loss function) was set to 0.0001, implying that training epochs would be repeated until the MSE was less than this number. A set of target network output values (i.e., training dataset) was obtained from DOE and was applied to calculate connection weights. The number of neurons in the hidden layer was adjusted from 1 to 20. MSE was computed to determine the optimal number of neurons. Table 5 shows the lowest mean MSE (0.00130) attained with 20 neurons in the hidden layer. As a result, the backpropagation ANN (4-20-1) model algorithm was selected for modelling.

Figure 8 ANN architecture (4-N₁-1)

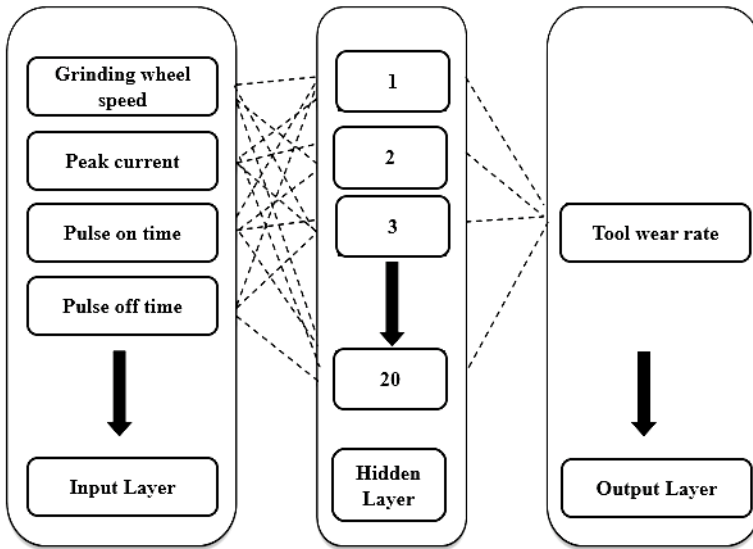


Table 5 Performance of ANN with the variation of neurons in the hidden layer

<i>Sr. no.</i>	<i>Number of neurons in hidden layer</i>	<i>MSE</i>
1	1	0.00510
2	2	0.00268
3	3	0.00221
4	4	0.00478
5	5	0.00276
6	6	0.00875
7	7	0.00950
8	8	0.00827
9	9	0.03550
10	10	0.00627
11	11	0.02825
12	12	0.02063
13	13	0.00885
14	14	0.02098
15	15	0.00319
16	16	0.00384
17	17	0.01210
18	18	0.00535
19	19	0.05282
20	20	0.00130

4.6 Validation experiments

Four new experiments were planned and carried out, each with a different setting of input process parameters, as shown in Table 6. Table 6 also shows the predicted TWR by RSM and ANN model and experimental output.

The experimental output values were compared with predicted values from RSM and ANN models, and it was also found that the ANN model provides a lower MSE of 0.018% than the RSM model MSE of 0.077%.

Table 6 Predicted TWR by RSM and ANN along with experimental results

<i>GWS</i> (rpm)	<i>I_p</i> (A)	<i>T_{on}</i> (μ s)	<i>T_{off}</i> (μ s)	RSM predicted (mm ³ /min)	ANN predicted (mm ³ /min)	Experimental output (mm ³ /min)
100	7	150	6	0.274	0.137	0.132
150	12	200	9	0.163	0.164	0.161
500	15	300	14	0.440	0.173	0.169
300	20	150	11	0.645	0.185	0.180

5 Conclusions

The goal of this study was to develop an accurate predictive model for TWR in the EDFG process while machining Monel-400. The experiments were carried out using the CCD design of the experiment technique, and the influence of input process parameters on TWR was investigated by ANOVA analysis. After that, RSM and ANN modelling techniques were used to make TWR predictions, which were then compared with validation experiments. The following conclusions were drawn from the study.

- 1 *GWS* and *I_p* both exhibited a very significant effect on TWR, with percentage contributions of 35.65 % and 24.39%, respectively.
- 2 There is a positive effect when the *GWS* increases from 200 to 600 rpm, resulting in lower TWR with a reduction of 61%.
- 3 Validation experiments performed shown that ANN had a better prediction accuracy as compared to RSM in predicting TWR. Therefore, ANN can be successfully applied for modelling complex processes such as EDFG.

References

- Abothula, B.C., Yadava, V. and Singh, G.K. (2010) 'Development and experimental study of electrodischarge face grinding', *Materials and Manufacturing Processes*, Vol. 25, No. 6, pp.482–487, <https://doi.org/10.1080/10426910903367436>.
- Davim, J.P., Gaitonde, V.N. and Karnik, S.R. (2008) 'Investigations into the effect of cutting conditions on surface roughness in turning of free machining steel by ANN models', *Journal of Materials Processing Technology*, Vol. 205, Nos. 1–3, pp.16–23, <https://doi.org/10.1016/j.jmatprotec.2007.11.082>.
- El-Taweel, T.A. (2009) 'Multi-response optimization of EDM with Al-Cu-Si-TiC P/M composite electrode', *International Journal of Advanced Manufacturing Technology*, Vol. 44, Nos. 1–2, pp.100–113, <https://doi.org/10.1007/s00170-008-1825-6>.

- Gouravaraju, S. et al. (2021) 'A Bayesian regularization-backpropagation neural network model for peeling computations', *Journal of Adhesion*, pp.1–32, <https://doi.org/10.1080/00218464.2021.2001335>.
- Gupta, I. and Tyagi, G. (2017) 'Optimization of machining parameters in electrical discharge machining process of Ti-6Al-4V alloy by Taguchi method', *International Journal of Production Engineering*, Vol. 3, No. 2, pp.44–50, <https://doi.org/10.37628/ijpe.v3i2.461>.
- Kumar, R. et al. (2017) 'Analysis and experimental study of electrical discharge face grinding on tungsten copper alloy', *10th Conference on Precision, Meso, Micro and Nano Engineering*, IIT Madras, Chennai, pp.680–685.
- Shoemaker, L.E. and Smith, G.D. (2006) 'Nickel: a century of innovation a century of monel metal: 1906–2006', *The Journal of The Minerals, Metals & Materials Society (JOM)*, September, Vol. 58, No. 9, pp.22–26, <https://doi.org/10.1007/s11837-006-0077-x>.
- Shu, K.M. and Tu, G.C. (2003) 'Study of electrical discharge grinding using metal matrix composite electrodes', *International Journal of Machine Tools and Manufacture*, Vol. 43, No. 8, pp.845–854, [https://doi.org/10.1016/S0890-6955\(03\)00048-8](https://doi.org/10.1016/S0890-6955(03)00048-8).
- Singh, G.K., Yadava, V. and Kumar, R. (2010) 'Diamond face grinding of WC-Co composite with spark assistance: experimental study and parameter optimization', *International Journal of Precision Engineering and Manufacturing*, Vol. 11, No. 4, pp.509–518, <https://doi.org/10.1007/s12541-010-0059-3>.
- Singh, S., Yadava, V. and Yadav, R.S. (2014) 'Development and experimental investigation of electro- discharge diamond face grinding', *5th International & 26th All India Manufacturing Technology, Design and Research Conference (AIMTDR 2014)*, IIT Guwahati, Assam, Guwahati, India, 12–14 December, pp.1–6.
- Tyagi, G., Gupta, I., Sharma, S.K.R. and Singh, G.K. (2017) 'Analysis and experimental study of electrical discharge face grinding on tungsten copper alloy', *International Journal of Production Engineering*, Vol. 3, No. 1, <https://doi.org/https://doi.org/10.37628/ijpe.v3i1.354>.
- Unune, D.R. and Mali, H.S. (2017) 'Parametric modeling and optimization for abrasive mixed surface electro discharge diamond grinding of Inconel 718 using response surface methodology', *International Journal of Advanced Manufacturing Technology*, Vol. 93, Nos. 9–1, pp.3859–3872, <https://doi.org/10.1007/s00170-017-0806-z>.
- Unune, D.R., Nirala, C.K. and Mali, H.S. (2019) 'Accuracy and quality of micro-holes in vibration assisted micro-electro-discharge drilling of Inconel 718', *Measurement: Journal of the International Measurement Confederation*, Vol. 135, pp.424–437, <https://doi.org/10.1016/j.measurement.2018.11.067>.
- Unune, D.R., Singh, V.P. and Mali, H.S. (2016) 'Experimental investigations of abrasive mixed electro discharge diamond grinding of nimonic 80A', *Materials and Manufacturing Processes*, Vol. 31, No. 13, pp.1718–1723, <https://doi.org/10.1080/10426914.2015.1090598>.
- Wu, K.L. et al. (2009) 'Study on the characteristics of electrical discharge machining using dielectric with surfactant', *Journal of Materials Processing Technology*, Vol. 209, No. 8, pp.3783–3789, <https://doi.org/10.1016/j.jmatprotec.2008.09.005>.
- Yadav, R.N. and Yadava, V. (2017) 'Experimental investigations of slotted electrical discharge abrasive grinding of Al/SiC/Gr composite', *Proceedings of the Institution of Mechanical Engineers, Part B: Journal of Engineering Manufacture*, Vol. 231, No. 6, pp.945–955, <https://doi.org/10.1177/0954405415579849>.
- Yadav, R.S., Singh, G. and Yadava, V. (2015) 'Experimental investigation of electro-discharge face grinding of metal matrix composite (Al/SiC)', *ELK Asia Pacific Journals – Special Issue*, Vol. 4, No. 1, pp.31–37, ISBN: 978-81-930411-4-7, <https://doi.org/10.16962/elkajp/si.arimpie-2015.31>.
- Youssefi, S., Emam-Djomeh, Z. and Mousavi, S.M. (2009) 'Comparison of artificial neural network (ANN) and response surface methodology (RSM) in the prediction of quality parameters of spray-dried pomegranate juice', *Drying Technology*, Vol. 27, No. 7, pp.910–917, <https://doi.org/10.1080/07373930902988247>.

Abbreviations

EDDG	electro discharge diamond grinding
<i>GWS</i>	grinding wheel speed
MRR	material removal rate
WWR	wheel wear rate
TWR	tool wear rate
CCD	central composite design
ANOVA	analysis of variance
MSE	mean square error.

Symbols

I_p	peak current
T_{on}	pulse on time
T_{off}	pulse off time
P	density of the workpiece.